Regular Article

PHYSICAL CHEMISTRY RESEARCH
Published by the
Iranian Chemical Society
www.physchemres.org
info@physchemres.org

Phys. Chem. Res., Vol. 12, No. 2, 305-320, June 2024

In Silico Studies on the Molecular Geometry, FMO, Mulliken Charges, MESP, ADME and Molecular Docking Prediction of Pyrogallol Carboxaldehydes as Potential Anti-tumour Agents

A. Ram Kumar[a], C. Senthamil Selvi[b], S. Selvaraj[c,*], G. P. Sheeja Mol[d] and P. Jayaprakash[e]

[a]*Department of Biotechnology, Saveetha School of Engineering, Saveetha Institute of Medical and Technical Sciences (SIMATS), Thandalam, Chennai, 602105, Tamil Nadu, India*

[b]*Department of Physics, S. A. Engineering College, Chennai, 600077, Tamil Nadu, India*

[c]*Department of Physics, Saveetha School of Engineering, Saveetha Institute of Medical and Technical Sciences (SIMATS), Thandalam, Chennai, 602105, Tamil Nadu, India*

[d]*PG Department of Physics, St. Joseph's College for Women, Alappuzha, 688001, Kerala, India, Affiliated to University of Kerala, Thiruvananthapuram, 695034, Kerala, India*

[e]*Department of Physics, St. Joseph's Institute of Technology, OMR, Chennai, 600119, Tamil Nadu, India*

(Received 21 December 2022, Accepted 29 July 2023)

In this study, quantum-chemical computational calculations were performed to evaluate the electronic structures of pyrogallol carboxaldehydes, specifically the pyrogallol-4-carboxaldehyde (P4C) and the pyrogallol-5-carboxaldehyde (P5C). To this end, the DFT/B3LYP/6-311++G(d,p) method and basis set were used. A comprehensive analysis of the structures and their chemical, biological, and various electronic features was done to gain deeper insights into the pyrogallol carboxaldehydes. Moreover, Mulliken population and molecular electrostatic potential surface (MESP) were calculated for comprehensive understanding of the bonding characteristics and reactive sites of the pyrogallol carboxaldehydes. The pharmacokinetic properties, including absorption, distribution, metabolism, and excretion (ADME) were assessed to predict the toxicity of the pyrogallol carboxaldehydes. Furthermore, *in silico* molecular docking was employed to determine the biological significance of the pyrogallol carboxaldehydes as potential anti-tumour agents. This was done by targeting oncogenic proteins such as Kristen rat sarcoma viral oncogene (K-RAS), Harvey rat sarcoma viral oncogene (H-RASGTP), and H-RASGDP, and the obtained binding energies were -5.46, -5.38, and -5.52 kcal mol^{-1} for the P4C and -5.53, -5.64, and -5.60 kcal mol^{-1} for the P5C, respectively.

Keywords: Pyrogallol carboxaldehydes, Anti-tumour agent, ADME, Molecular docking, DFT, Oncogenic proteins

INTRODUCTION

In recent decades, there have been many studies on the biological, structural, and spectroscopic properties of the derivatives of aldehydes and benzaldehydes, which are used in pharmaceutical, agrochemical and dye industries and also used as intermediate in the processing of flavours. The most well-known natural source of benzaldehyde is the primary component of essential oils that may be extracted from the pits of various fruits such as peaches, cherries, and apricots through the process of pressing [1]. The derivatives of aldehydes have been used as enzyme inhibitors, free radical scavenging antioxidants, and in industries for the manufacturing of polymers and coumarin [2-5]. In some cases, the derivatives of benzaldehyde are used as an anti-cancer agent by inhibiting cytochrome P450 and inducing lipid peroxidation in cancer cells [6]. The theoretical and experimental studies on benzaldehyde derivatives such as

*Corresponding author. E-mail: selvarajs.sse@saveetha.com

syringaldehyde, 4-hydroxy-3-methoxycinnamaldehyde, and 5-(hydroxymethyl)-2-furaldehyde have been reported earlier [7-9]. Most of the time, carboxaldehydes are prepared by oxidizing primary alcohols or aldehydes. The pyrogallol-4-carboxaldehyde (P4C) and pyrogallol-5-carboxaldehyde (P5C) are aromatic, phenolic, and aldehyde compounds having a benzene ring structure that has been replaced with hydroxyl and aldehyde groups. From the structure point of view, the P4C has three hydroxyl groups (-OH) in *ortho, meta,* and *para* positions concerning the aldehyde group, while in the P5C, those hydroxyl groups are attached to *meta* and *para* positions with the molecular formula of $C_7H_6O_4$ and molecular weight of 154.12 g mol^{-1}. One of the pyrogallol carboxaldehyde, the P4C, is an essential intermediate in the production of antiparkinson medication benserazide, which is a peripheral dopa decarboxylase inhibitor [10]. Another pyrogallol carboxaldehyde, the P5C, is isolated from *Geum japonicum* and has potent antioxidant activity [11].

Cancer has claimed the lives of 10 million people globally in recent decades, making it one of the leading causes of death. Lung and breast cancers are the most common kinds of cancer in men and women [12], and they are caused by lifestyle, hormonal medicines, ageing, and chemical exposure. Currently, oncogenes serve as a main molecular target for the development of novel anti-cancer drugs. A mutated variant of a normal gene (a proto-oncogene) that has the potential to promote the development of cancer is an oncogene. The term "oncogene" was coined to characterize genes that, when activated or overexpressed as a result of mutations, can promote uncontrolled cell proliferation, and contribute to the formation of tumours. The phosphoinositol-3-kinase (PI3K), rat sarcoma (Ras), tumour protein53 (p53), phosphatase and tensin homolog (PTEN), and retinoblastoma protein (Rb) are some of the oncogenes and tumour suppressor genes that are frequently altered in cancer cells. Nonetheless, it appears that a large number of low-frequency alterations can contribute to oncogenesis [13]. Over the past few decades, there has been a notable surge toward using computational methods to understand the chemical characteristics of compounds in the field of pharmacy, pharmacology and drug designing without solely depending on experimental procedures. Density functional Theory (DFT) a theoretical computational approach, stands out as a precise, cost-effective, flexible, and more dependable approach compared to other quantum-chemical methods used to predict the molecular structures of compounds [14-19]. A survey of the literature revealed that the P4C and P5C have not been subjected to any *in silico* studies. Bearing this idea in mind, the present study focuses on detailed analysis of the electronic, structural, pharmacokinetics and biological properties of pyrogallol carboxaldehydes. To the best of our knowledge, this is the first-time that quantum-chemical and molecular docking computational methods are used for mentioned analysis.

MATERIALS AND METHODS

Computational Methods

The quantum-chemical calculations of pyrogallol carboxaldehydes were performed using the density functional theory (DFT), Becke's three parameters Lee-Yang-Parr (B3LYP) DFT/B3LYP/6-311++G(d,p) level of theory and Gaussian 09W program, without any limitation on geometry [20-23]. The optimized geometrical parameters and electronic properties of pyrogallol carboxaldehydes were visualized by the Chemcraft program [24]. The Molinspiration Cheminformatics online tool (https://www.molinspiration.com/cgi-bin/properties) was utilized to screen the ADME (absorption, distribution, metabolism, and excretion) properties of the title ligand molecules, and the potential targets were predicted using Swiss Target Prediction [25]. The crystal structure of oncogenic proteins such as Kristen rat sarcoma viral oncogene (K-RAS), Harvey rat sarcoma viral oncogene (H-RASGTP), and H-RASGDP with PDB IDs of 4DSU, 5P21, and 4Q21 with a resolution of 2, 1.35, and 1.7 Å was retrieved from Research Collaboratory for Structural Bioinformatics (RCSB) Protein Data Bank (PDB) and was used as the target, accordingly. The heteroatoms, bound ligands and water molecules were removed from the crystal structures using the PyMOL graphics tool [26]. The structure of pyrogallol carboxaldehydes was built by using GaussView 6.0 program [27] and it was converted into a PDB file format to refine as a ligand. AutoDock was used for molecular docking studies [28], and for virtual screening of the 2D protein-ligand interaction, binding energy, hydrogen bonding and hydrophobic interaction were calculated using LigPlot$^+$ program [29].

RESULTS AND DISCUSSION

Molecular Geometry

The optimized molecular structure of pyrogallol carboxaldehydes is shown in Fig. 1. The atomic numberings and the geometrical parameters (bond lengths and bond angles) are presented in Tables 1 and 2. The calculated values for the P4C were compared with the experimental values available in the literature [30]. However, the experimental data for the P5C was not available in the literature, so it was

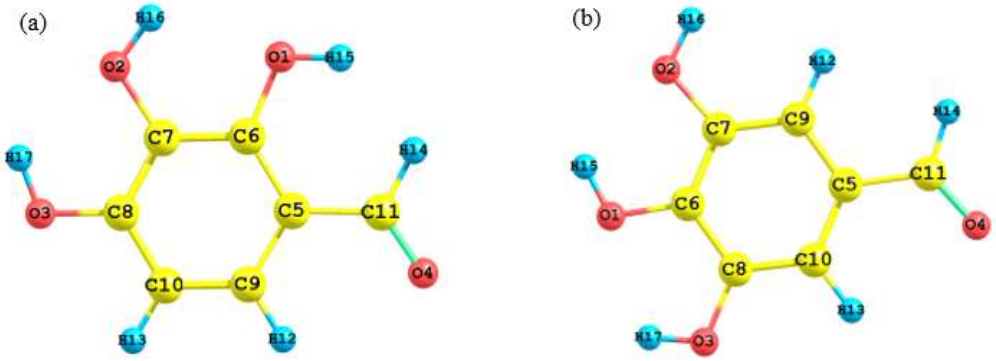

Fig. 1. Optimized molecular structure of (a) P4C and (b) P5C in the gas phase.

Table 1. Experimental and Theoretical Geometrical Parameters of P4C

Bond lengths (Å)	Theoretical	Experimental[a]	Bond lengths (Å)	Theoretical	Experimental[a]
O_1-C_6	1.372	1.364	C_5-C_{11}	1.464	1.425
O_1-H_{15}	0.962	0.841	C_6-C_7	1.392	1.366
O_2-C_7	1.371	1.372	C_7-C_8	1.396	1.402
O_2-H_{16}	0.966	0.839	C_8-C_{10}	1.400	1.398
O_3-C_8	1.353	1.350	C_9-C_{10}	1.380	1.373
O_3-H_{17}	0.967	0.827	C_9-H_{12}	1.083	0.948
O_4-C_{11}	1.214	1.252	C_{10}-H_{13}	1.082	0.948
C_5-C_6	1.409	1.415	C_{11}-H_{14}	1.116	0.949
C_5-C_9	1.409	1.410	-	-	-
Bond angles (◦)	**Theoretical**	**Experimental[a]**	**Bond angles (◦)**	**Theoretical**	**Experimental[a]**
C_6-O_1-H_{15}	111.6	114.3	C_6-C_5-C_{11}	122.1	121.9
O_1-C_6-C_5	125.9	120.3	C_5-C_6-C_7	120.3	121.5
O_1-C_6-C_7	113.8	118.1	C_9-C_5-C_{11}	119.7	119.6
C_7-O_2-H_{16}	109.1	110.0	C_5-C_9-C_{10}	121.6	120.4
O_2-C_7-C_6	122.5	117.9	C_5-C_9-H_{12}	117.5	119.7
O_2-C_7-C_8	117.2	123.0	C_5-C_{11}-H_{14}	116.2	117.9
C_8-O_3-H_{17}	108.8	116.0	C_6-C_7-C_8	120.3	118.9
O_3-C_8-C_7	120.2	121.1	C_7-C_8-C_{10}	120.1	120.8
O_3-C_8-C_{10}	119.8	118.0	C_8-C_{10}-C_9	119.4	119.8
O_4-C_{11}-C_5	125.5	124.1	C_8-C_{10}-H_{13}	118.8	119.9
O_4-C_{11}-H_{14}	118.3	117.8	C_{10}-C_9-H_{12}	120.8	119.7
C_6-C_5-C_9	118.2	118.4	C_9-C_{10}-H_{13}	121.8	120.1

[a]Taken from Ref. [30].

Table 2. Experimental and Theoretical Geometrical Parameters of P5C

Bond lengths (Å)	Theoretical	Experimental[a]	Bond lengths (Å)	Theoretical	Experimental[a]
O_1-C_6	1.364	1.357	C_5-C_{11}	1.477	1.473
O_1-H_{15}	0.966	0.839	C_6-C_7	1.395	1.402
O_2-C_7	1.376	1.362	C_6-C_8	1.402	1.394
O_2-H_{16}	0.962	0.892	C_7-C_9	1.387	1.388
O_3-C_8	1.359	1.373	C_8-C_{10}	1.387	1.388
O_3-H_{17}	0.966	0.879	C_9-H_{12}	1.086	0.949
O_4-C_{11}	1.211	1.242	C_{10}-H_{13}	1.082	0.950
C_5-C_9	1.402	1.402	C_{11}-H_{14}	1.112	-
C_5-C_{10}	1.399	1.398	-	-	-
Bond angles (°)	Theoretical	Experimental[a]	Bond angles (°)	Theoretical	Experimental[a]
C_6-O_1-H_{15}	109.2	108.0	C_9-C_5-C_{11}	118.7	119.6
O_1-C_6-C_7	122.2	121.1	C_5-C_9-C_7	119.3	118.8
O_1-C_6-C_8	117.4	118.8	C_5-C_9-H_{12}	120.2	120.6
C_7-O_2-H_{16}	110.8	110.9	C_{10}-C_5-C_{11}	120.5	119.4
O_2-C_7-C_6	114.6	114.3	C_5-C_{10}-C_8	119.6	119.6
O_2-C_7-C_9	125.2	125.0	C_5-C_{10}-H_{13}	120.1	120.2
C_8-O_3-H_{17}	108.9	110.1	C_5-C_{11}-H_{14}	114.3	-
O_3-C_8-C_6	120	121.0	C_7-C_6-C_8	120.4	119.9
O_3-C_8-C_{10}	120.3	118.8	C_6-C_7-C_9	120.1	120.5
O_4-C_{11}-C_5	125.3	123.6	C_6-C_8-C_{10}	119.7	120.0
O_4-C_{11}-H_{14}	120.4	-	C_7-C_9-H_{12}	120.5	120.5
C_9-C_5-C_{10}	120.8	120.9	C_8-C_{10}-H_{13}	120.3	120.1

[a]Taken from Ref. [31].

compared with a structurally similar compound (3,4,5-tri hydroxybenzoic acid) [31]. The pyrogallol carboxaldehydes have four types of prominent bond lengths which are 4 O-C, 3 O-H, 7 C-C, and 3 C-H bonds, and four prominent bond angles which are 3 C-O-H, 7 O-C-C, 8 C-C-C, and 6 C-C-H.

The optimized bond lengths of the hydroxyl (-OH) groups were theoretically simulated in the range of 0.962-0.967 and 0.962-0.966 Å, and the corresponding experimental values are in the range of 0.827-0.841 Å and 0.839-0.892 Å for P4C and P5C, respectively. At the same time, the bond lengths of C-H were theoretically simulated in the range of 1.082-1.116 and 1.082-1.112 Å, which experimentally observed in the range of 0.948-0.949 and 0.949-0.950 Å for the P4C and P5C, respectively. The bond lengths of C-O were theoretically simulated in the range of1.214-1.372 and 1.211-1.376 Å, and the corresponding experimental values lie in the range of 1.252-1.372 and 1.242-1.373 Å for the P4C and P5C, respectively. It is evident that the double-bonded CO of the aldehyde group has less bond length when comparing it to the other single-bonded CO of the aromatic ring. The calculated bond lengths of C-C in the ring structure were in the range of 1.380-1.409 Å for the P4C and 1.387-1.402, and the corresponding experimental values were in the range of 1.366-1.415 Å for the P4C and 1.388-1.402 Å for the P5C. This shows that the experimental bond lengths of C-C are in good agreement with the theoretical simulations. In particular, the bond length of C_5-C_{11} were 1.464 and 1.477 Å and the experimental values

were 1.425 and 1.473 Å for the P4C and P5C, respectively. It is obvious that the influence of the electronegative oxygen atom resulted in an increase in the bond length of the C_5-C_{11}. On the other hand, oxygen (O_4) is capable of taking electrons away from carbon (C_{11}), which made the bond longer and weaker.

The bond angle of the aldehyde group (O_4-C_{11}-H_{14}) was theoretically calculated at 118.3 and 120.4° for P4C and P5C and the experimental value was 117.8° for P4C. The C-OH bond angle was theoretically calculated in the range of 108.8-111.6 and 108.9-110.8° and experimentally observed in the range of 110.0-116.0 and 108.0-110.9 ° for the P4C and P5C, respectively. The bond angle of endocyclic carbon (C=C) atoms was theoretically calculated in the range of 118.2-121.6 and 119.3-120.8° and experimentally observed in the range of 118.4-121.5° and 118.8-120.9° for the P4C and P5C, correspondingly. The bond angles of C_6-C_5-C_{11} and C_9-C_5-C_{11} were theoretically calculated at 122.1, 119.7° and experimentally observed at 121.9, 119.6° for the P4C. Similarly, for P5C, the aforementioned bond angles were theoretically calculated at 118.7° and 120.5° and experimentally observed at 119.6° and 119.4°. In the case of P4C, the bond angles of O-C-C, C-C-H were theoretically calculated in the ranges of 113.8-125.9 and 116.2-121.8°, and experimentally observed in the ranges of 117.9-124.1 and 117.9-120.1°. Also, for the P5C, the respective bond angles were theoretically calculated in the ranges of 114.6-125.2° and 114.3-120.5° and experimentally observed at the ranges of 114.3-123.6° and 120.2-120.6°. The optimized simulated values exhibit a remarkable coincidence with the experimental values, with linear coefficient values (R^2) of 0.9738 for the bond length and 0.58552 for the bond angles for P4C. Similarly, for P5C, the linear coefficient values of 0.97769 for the bond length and 0.96352 for the bond angles were calculated; the correlation graph between the simulated and observed values are shown in Figs. S1 and S2 (Supplementary Material).

Frontier Molecular Orbitals

The frontier molecular orbital (FMO), chemical softness, chemical hardness, chemical potential, electronegativity, and electron affinity of the pyrogallol carboxaldehydes have been simulated in the gas phase and the optical and electronic properties are reported in Table 3 [32,33]. In the gas phase, the highest occupied molecular orbital (HOMO) and lowest unoccupied molecular orbital (LUMO) of the pyrogallol carboxaldehydes had energy values of -6.6159 eV and -6.6346 eV for the P4C, and -2.1096 eV and 1.97258 eV f or the P5C, respectively. In Figs. 2 and 3, the red and green colours represent the positive and negative sites of the

Table 3. Frontier Molecular Analysis of Pyrogallol Carboxaldehydes

Parameters	Formula	P4C	P5C
E_{HOMO} (eV)	-	-6.6159	-6.6346
E_{HOMO-1} (eV)	-	-6.9348	-5.6028
E_{LUMO} (eV)	-	-2.1096	-1.9725
E_{LUMO+1} (eV)	-	-0.9632	-0.9858
$E_{HOMO-LUMO}$ gap (eV)	-	4.5063	4.6621
Ionization potential (I)	$-E_{HOMO}$	6.6159	6.6346
Electron affinity (A)	$-E_{LUMO}$	2.1096	1.9725
Electronegativity (χ)	(I+A)/2	4.3627	4.3035
Chemical potential (μ)	-χ	-4.3627	-4.3035
Chemical hardness (η)	I-A	4.5063	4.6621
Chemical softness (s)	1/2η	0.1109	0.1072
Global electrophilicity (ω)	$\mu^2/2\eta$	2.1118	1.9862
Maximum electron charge (ΔN_{max})	-(μ/η)	0.9681	0.9230

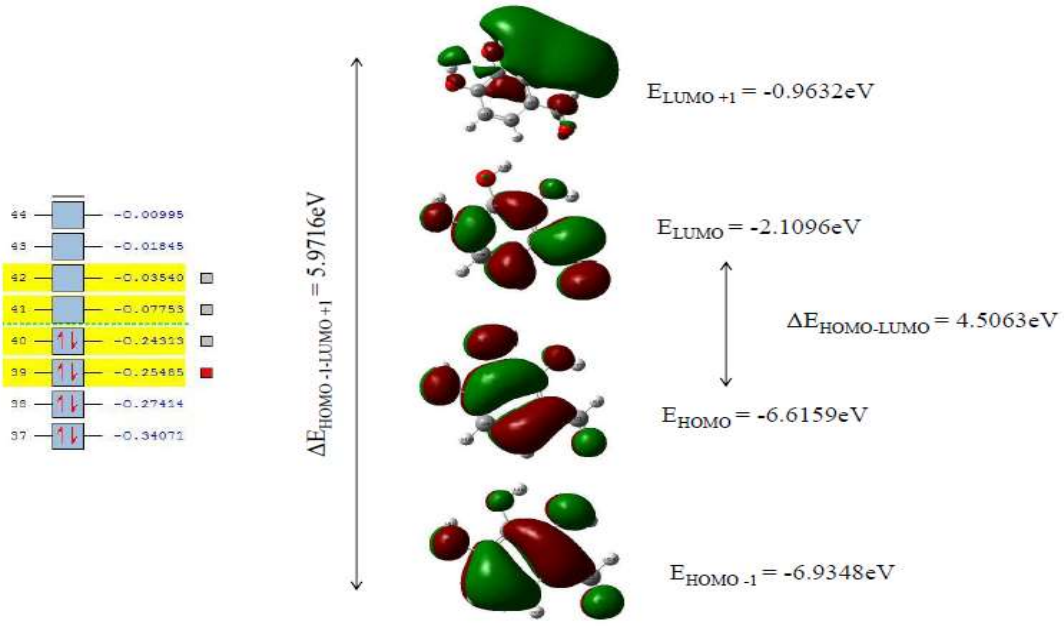

Fig. 2. The HOMO-LUMO plots of P4C.

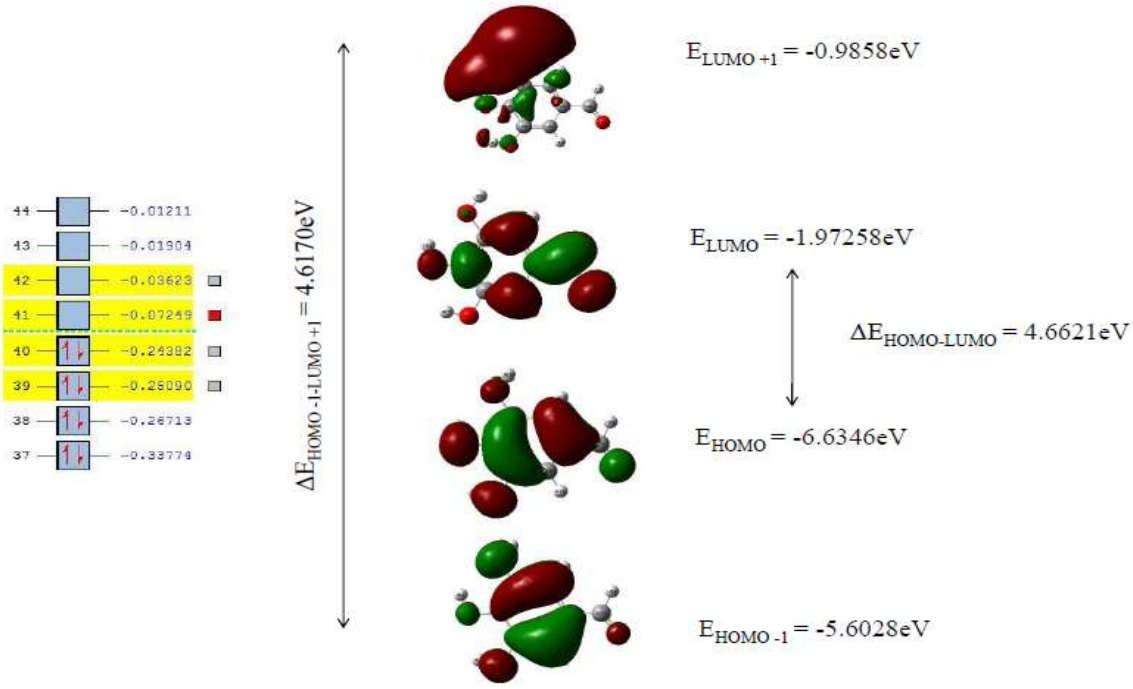

Fig. 3. The HOMO-LUMO plots of P5C.

pyrogallol carboxaldehydes, respectively. It was observed that the HOMO was localized over the ring structure and hydroxyl group. On the other hand, LUMO was localized over the ring structure as well as the aldehyde group. The energy gap calculated in the gas phase was 4.5063 eV for the P4C and 4.6621 eV for the P5C. The P4C exhibited a lower

energy gap, indicating the occurrence of charge transfer within the molecule, which was clearly evidenced by the Density of States (DOS) spectra, as visualized in Figs. 4 and 5. A molecule with a higher electrophilicity index can act as an electrophilic species and exhibit stronger binding affinity to biomolecules. Additionally, a molecule with a low chemical hardness value and a highly negative chemical potential value is considered a soft molecule, indicating high polarizability. In the present study, the chemical hardness and chemical potential values were around 4.5063 and -4.3627 for the P4C, and 4.6621 and -4.3035 for the P5C, respectively. This is an evident of the high polarizability and potent bio-activeness of the pyrogallol carboxaldehydes. Moreover, the P4C had higher levels of polarizability and chemical reactivity compared to the P5C. The global reactivity of the P4C was 2.1118 eV, which was higher than the corresponding value (1.9862 eV) for the P5C. Similarly, the chemical hardness and chemical potential value was around 4.5063 and -4.3627 for the P4C, and 4.6621 and -4.3035 for the P5C, respectively.

Mulliken Population Analysis

In quantum-chemical calculations, the Mulliken atomic charge distribution is an extremely important factor to consider when attempting to evaluate the electronic properties and chemical reactivity of molecules. This is because the charges on atoms can influence polarizability, dipole moment, electronic structure, and a variety of other molecular aspects [34]. The Mulliken atomic charges of the P4C and the P5C are presented in Table 4 and visualized in Fig. S3 (Supplementary Material). In the both compounds, the C_5 atom attached to the aldehyde group (-CHO) and the carbon atom at *para* position showed high positive values when comparing to other carbon atoms. On the other hand, the C_6 (-1.02777 e) and C_7 (-0.30054 e) atoms attached to the hydroxyl (-OH) group showed highly negative values for the P4C. Also, the C_9 (-1.01239 e) atom had more negative values than another carbon atoms of the P5C. The proximity of the aldehyde and the hydroxyl group influenced the charges of the carbon atoms. As expected, all the hydrogen atoms were positivity charged and all the oxygen atom showed negative charge, which was also confirmed by the molecular electrostatic potential (MESP) surfaces.

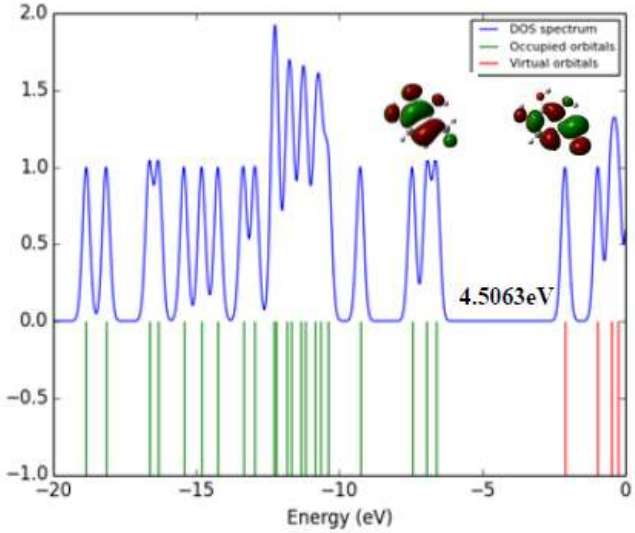

Fig. 4. Density of states (DOS) spectrum of P4C.

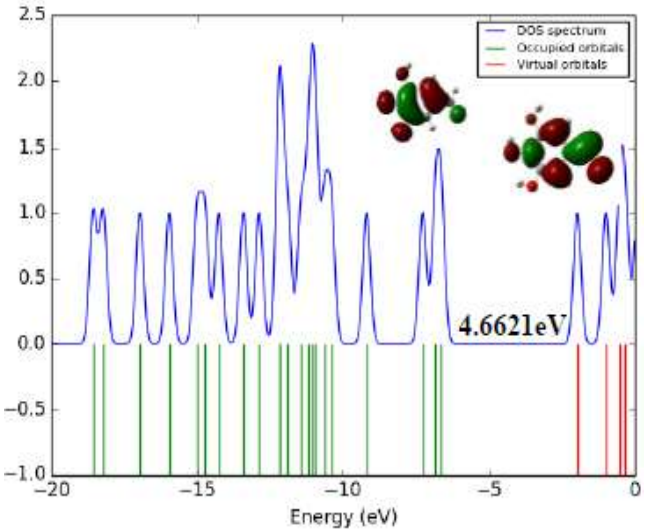

Fig. 5. Density of states (DOS) spectrum of P5C

Molecular Electrostatic Potential Surface

Molecular electrostatic potential surfaces (MESP) were utilized to determine the nucleophilic and electrophilic regions. As illustrated in Fig. 6, those regions of the pyrogallol carboxaldehydes were shown by the variation of colour bands, which was predicted between -8.104×10^{-2} to 8.104×10^{-2} e.s.u for the P4C, and -8.138×10^{-2} to 8.138×10^{-2} e.s.u for the P5C.

Table 4. Mulliken Population Analyses of Pyrogallol Carboxaldehydes

Atoms	P4C	P5C
O_1	-0.25891	-0.30201
O_2	-0.30869	-0.31162
O_3	-0.23664	-0.24244
O_4	-0.27049	-0.24445
C_5	1.38222	1.234303
C_6	-1.02777	0.081555
C_7	-0.30054	-0.07842
C_8	0.13328	-0.37569
C_9	0.01594	-1.01239
C_{10}	-0.31723	-0.04264
C_{11}	-0.11558	-0.02422
H_{12}	0.19746	0.108414
H_{13}	0.19526	0.207403
H_{14}	0.04892	0.125606
H_{15}	0.27256	0.299814
H_{16}	0.29794	0.287320
H_{17}	0.29224	0.289473

From the above figure, the white colour around the hydrogen atoms shows the electron-poor region, which are the binding sites for the electrophile reactive species. The hydroxyl hydrogen atoms showed more positive potential than the hydrogen atoms. The red colour around the oxygen atoms shows the electron-rich region, which are the binding sites for the nucleophilic reactive species. The red colour region around the oxygen atoms in the hydroxyl and aldehyde group are the binding site for the nucleophilic reactive species. The *ortho*-position carbon atoms showed more negative potential due to the proximity of the aldehyde group. These results are in good agreements with the Mulliken population analyses.

ADME Prediction

The ADME of the pyrogallol carboxaldehydes was predicted using the Molinspiration Cheminformatics toolkit, which is presented in Table 5. Lipinski's rule of five says that a compound is biologically active if it has fewer than 5 hydrogen bond donors and 10 hydrogen bond acceptors, a

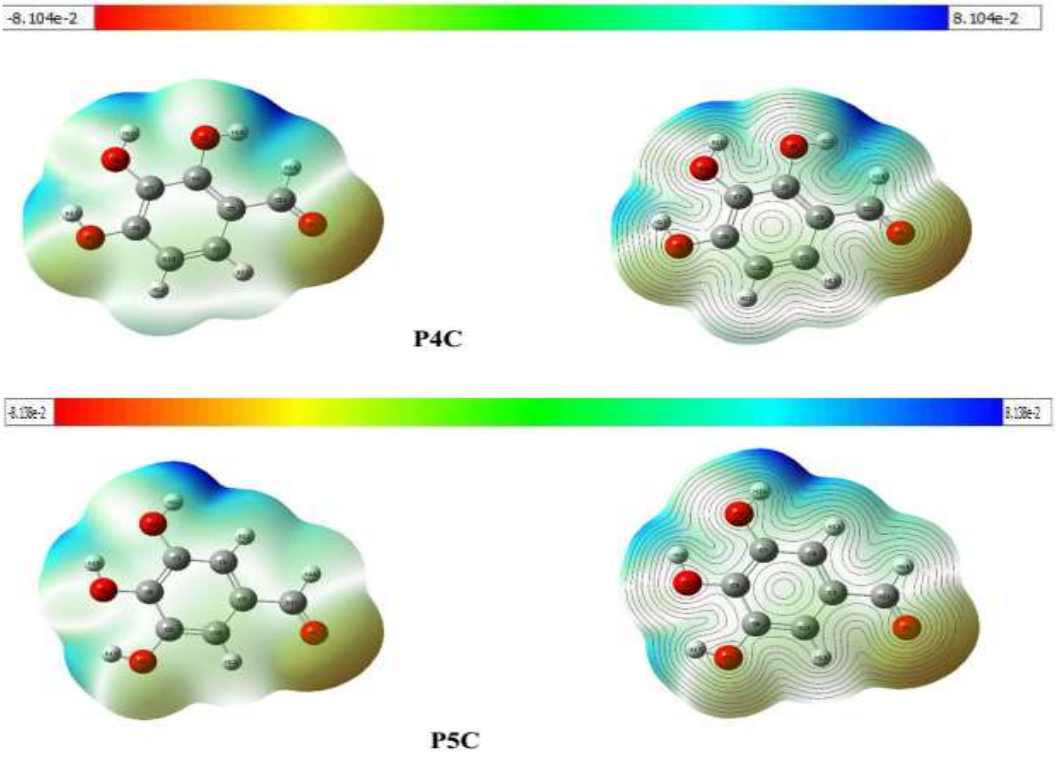

Fig. 6. The total electron density (left) and the contour map (right) with the molecular electrostatic potential surface of pyrogallol carboxaldehydes.

Table 5. The ADME Prediction of Pyrogallol Carboxaldehydes

Parameters	P4C	P5C
Formula	$C_7H_6O_4$	$C_7H_6O_4$
Molecular weight	154.12 g mol^{-1}	154.12 g mol^{-1}
Number of heavy atoms	11	11
Number of aromatic heavy atoms	6	6
Fraction Csp^3	0.00	0.00
Number of rotatable bonds	1	1
Number of hydrogen bond acceptors	4	4
Number of hydrogen bond donors	3	3
Molar refractivity	37.90	37.90
TPSA (Topological polar surface area)	77.76 $Å^2$	77.76 $Å^2$
Lipophilicity		
$LogP_{o/w}$	0.50	0.35
Water solubility		
Log	-1.68	-1.54
Solubility	32.1 mg ml^{-1}	44.8 mg ml^{-1}
Absorption		
GI	High	High
Distribution		
BBB permeation	No	No
P-gp substrate	No	No
Metabolism		
CYP1A2 inhibitor	No	No
CYP2C19 inhibitor	No	No
CYP2C9 inhibitor	No	No
CYP2D6 inhibitor	No	No
CYP3A4 inhibitor	Yes	Yes
LogKp (skin permeation)	-6.62 cm s^{-1}	-6.79 cm s^{-1}
Drug-likeness		
Lipinski	0	0
Ghose	3	3
Veber	Yes	Yes
Medicinal chemistry		
PAINS	1	1
Brenk	2	2
Leadlikeness	No	No
Synthetic accessibility	1.12	1.01
Bioavailability score	0.55	0.55

molecular weight of less than 500 g mol^{-1}, a miLogP value of 5 or less, and no more than one violation of any of these four rules. Here, the pyrogallol carboxaldehydes have 3 hydrogen bond donors and 4 hydrogen bond acceptors, the molecular weight is less than 500 g mol^{-1}, and the miLogP value is 0.70 (P4C) and 0.47 (P5C). From these findings, both of these have possibilities to be biologically active compounds. The pharmacokinetic behaviours of the gastrointestinal absorption and brain access are the two chemical aspects that need to be evaluated at various phases of the drug development technique. The BOILED-Egg method was used to investigate the gastrointestinal (GI) absorption and blood-brain barrier (BBB), human intestinal absorption (HIA), and P-glycoprotein (PGP) permeability capabilities using SwissADME prediction [35]. According to Fig. 7, the pyrogallol carboxaldehydes were overlapped at the same point and actively absorbed by the gastrointestinal and were not able to penetrate the blood-brain barrier. The list of the potential biological targets for the pyrogallol carboxaldehydes is presented in Tables 6 and 7, and also illustrated in Fig. 8. Based on the obtained results, it became evident that the P4C exhibited a 80% probability of inhibition for transferase, 13.3% for lyases, and 6.7% for enzymes.

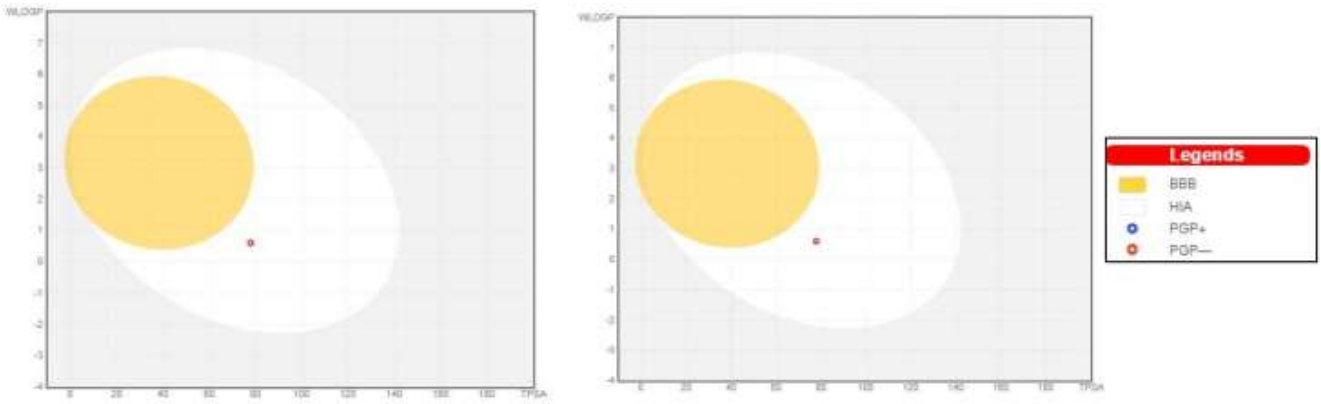

Fig. 7. Boiled egg model of P4C (left) and P5C (right).

Table 6. Biological Target List for P4C

Target name	Common name	Uniport ID	chEMBL ID	Class
Cathechol O-methyltransferase	COMT	P21964	CHEMBL2023	Transferase
Carbonic anhydrase II	CA2	P00918	CHEMBL205	Lyase
Carbonic anhydrase VII	CA7	P43166	CHEMBL2326	Lyase
Carbonic anhydrase I	CA1	P00915	CHEMBL261	Lyase
Carbonic anhydrase III	CA3	P07451	CHEMBL2885	Lyase
Carbonic anhydrase VI	CA6	P23280	CHEMBL3025	Lyase
Carbonic anhydrase XII	CA12	O43570	CHEMBL3242	Lyase
Carbonic anhydrase XIV	CA14	Q9ULX7	CHEMBL3510	Lyase
Carbonic anhydrase IX	CA9	Q16790	CHEMBL3594	Lyase
Alpha-(1,3)-fucosyltransferase 7	FUT7	Q11130	CHEMBL3596077	Transferase
Carbonic anhydrase IV	CA4	P22748	CHEMBL3729	Lyase
Carbonic anhydrase XIII	CA13	Q8N1Q1	CHEMBL3912	Lyase
Carbonic anhydrase VB	CA5B	Q9Y2D0	CHEMBL3969	Lyase
Carbonic anhydrase VA	CA5A	P35218	CHEMBL4789	Lyase
Serine/threonine protein Kinase/endoribonuclease	ERN1	O75460	CHEMBL1163101	Enzyme

Table 7. Biological Target List for P5C

Target name	Common name	Uniport ID	chEMBL ID	Class
Cathechol O-methyltransferase	COMT	P21964	CHEMBL2023	Transferase
Carbonic anhydrase VII	CA7	P43166	CHEMBL2326	Lyase
Carbonic anhydrase I	CA1	P00915	CHEMBL261	Lyase
Carbonic anhydrase III	CA3	P07451	CHEMBL2885	Lyase
Carbonic anhydrase VI	CA6	P23280	CHEMBL3025	Lyase
Carbonic anhydrase XIV	CA14	Q9ULX7	CHEMBL3510	Lyase
Alpha-(1,3)-fucosyltransferase 7	FUT7	Q11130	CHEMBL3596077	Transferase
Carbonic anhydrase IV	CA4	P22748	CHEMBL3729	Lyase
Carbonic anhydrase XIII	CA13	Q8N1Q1	CHEMBL3912	Lyase
Carbonic anhydrase VB	CA5B	Q9Y2D0	CHEMBL3969	Lyase
Carbonic anhydrase VA	CA5A	P35218	CHEMBL4789	Lyase
Tyrosinase	TYR	P14679	CHEMBL1973	Oxidoreductase
Carbonic anhydrase II	CA2	P00918	CHEMBL205	Lyase
Carbonic anhydrase XII	CA12	O43570	CHEMBL3242	Lyase
Carbonic anhydrase IX	CA9	Q16790	CHEMBL3594	Lyase

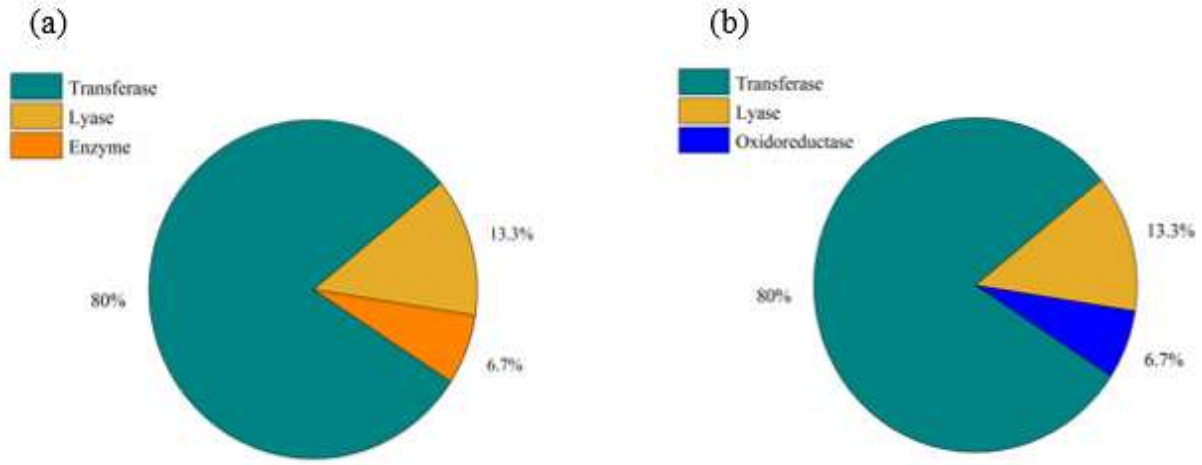

Fig. 8. Percentage distribution of biological target for (a) P4C and (b) P5C

Conversely, the P5C showed a 80% inhibitor probability for transferase, 13.3% for lyases, and 6.7% for oxidoreductases. The overall results show that the pyrogallol carboxaldehydes obey the Lipinski's criterion, indicating their potential bioavailability.

Molecular Docking

The molecular-docking approach is used to study the interactions of various chemical species with various biological macromolecules, creating a potential new medicine. In molecular-docking analysis, the primary objective is to attain the lowest energy and inhibition constant, as these factors hold immense significance [36,37]. Bearing this idea in mind, a molecular docking study was performed on oncogenic proteins such as K-RAS, H-RASGTP, and H-RASGDP, which are visualized in Fig. 9.

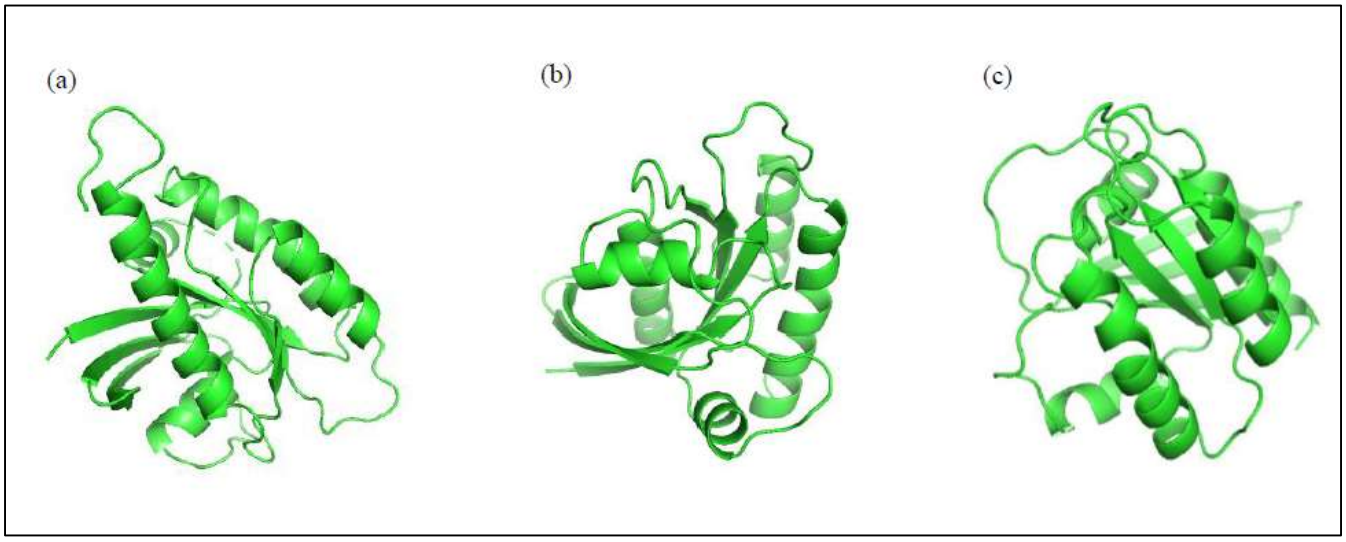

Fig. 9. The PyMOL view of target proteins (a) 4DSU, (b) 4Q21 and (c) 5P21.

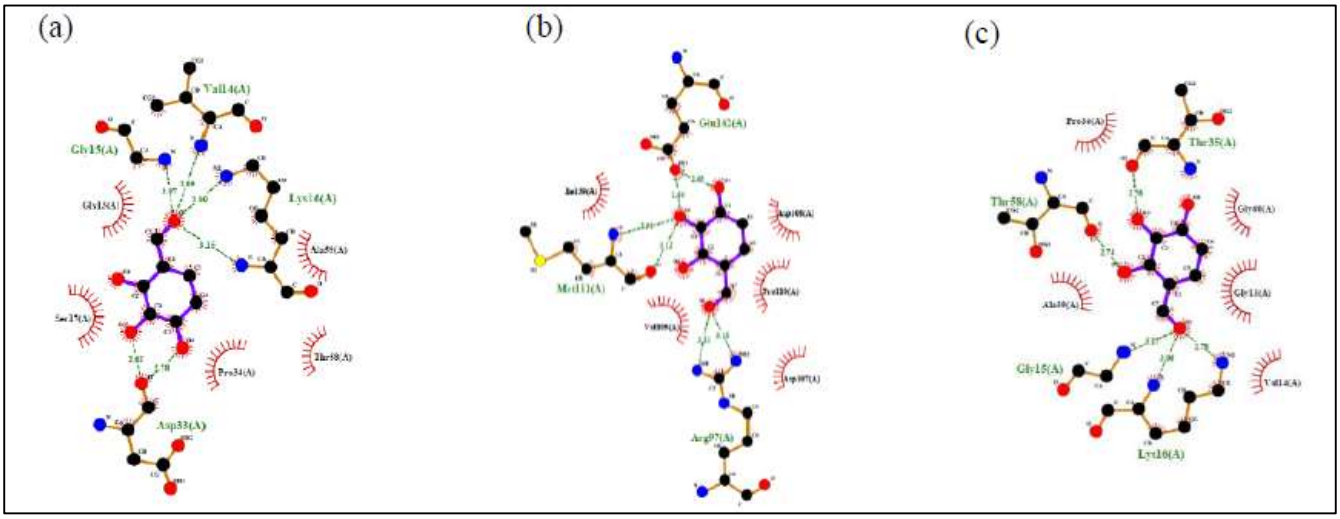

Fig. 10. The 2D LigPlot+ view of P4C against (a) 4DSU, (b) 4Q21 and (c) 5P21.

The values of hydrogen bonding, hydrophobic interaction and binding energy between the title ligands and proteins are reported in Table 8, and schematically represented in Figs. 10 and 11. Here, the ligand P4C showed binding energy of -5.46, -5.52 and -5.38 kcal mol^{-1} for binding to the target proteins 4DSU, 4Q21, and 5P21, respectively. The P4C-4DSU complex formed six hydrogen bonds through active sites of The values of hydrogen bonding, hydrophobic interaction and binding energy between the title ligands and proteins are reported in Table 8, and schematically represented in Figs. 10 and 11. Here, the ligand P4C showed binding energy of -5.46, -5.52 and -5.38 kcal mol^{-1} for binding to the target proteins 4DSU, 4Q21, and 5P21, respectively. The P4C-4DSU complex formed six hydrogen bonds through active sites of the aliphatic amino acids such as glycine (3.07 Å), valine (2.99 Å), lysine (2.89, 3.15 Å) and asparagine (2.62, 2.78 Å). Also, the hydrophobic interactions occurred between the aliphatic and the heterocyclic amino acids such as glycine, serine, threonine, alanine, and proline. In a similar way, the P4C-4Q21 complex formed six hydrogen bonds through the

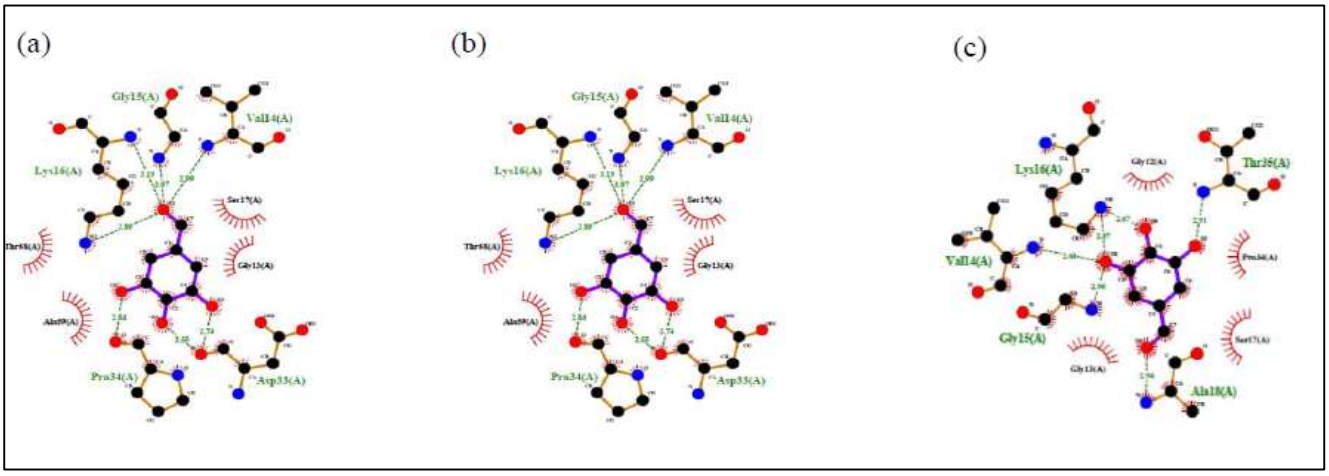

Fig. 11. The 2D LigPlot^{+} view of P5C against (a) 4DSU, (b) 4Q21 and (c) 5P21.

Table 8. Molecular Docking Studies of Pyrogallol Carboxaldehydes

Ligand	Protein	Binding score	Hydrogen bonding	Bond distance (Å)	Hydrophobic interactions
P4C	4DSU	-5.46	Glycine 15 Valine 14 Lysine 16 Asparagine 33	3.07 2.99 2.89, 3.15 2.62, 2.78	Glycine 13 Serine 17 Proline 34 Threonine 58 Alanine 59
	4Q21	-5.52	Methionine 111 Arginine 97 Glutamic acid 162	3.12, 2.90 3.15, 3.33 2.65, 2.64	Isoleucine 139 Valine 109 Asparagine 107 Proline 110 Asparagine 108
	5P21	-5.38	Threonine 35 Threonine 58 Glycine 15 Lysine 16	2.76 2.74 3.17 3.06, 2.78	Proline 34 Alanine 59 Glycine 13 Glycine 60 Valine 14
P5C	4DSU	-5.53	Glycine 15 Lysine 16 Proline 34 Asparagine 33 Valine 14	3.07 2.89, 3.15 2.84 2.55, 2.74 2.99	Glycine 13 Serine 17 Threonine 58 Alanine 59
	4Q21	-5.60	Glycine 15 Lysine 16 Valine 29 Glycine 13 Tyrosine 32	2.94 2.93 2.93 3.21 2.90, 3.0, 2.60	Valine 14 Serine 17 Proline 34 Alanine 18 Glutamic acid 31
	5P21	-5.64	Lysine 16 Valine 14 Glycine 15 Alanine 18 Threonine 35	2.87, 2.67 2.68 2.98 2.94 2.91	Glycine 13 Serine 17 Proline 34 Glycine 12

active sites of the aliphatic amino acids such as methionine (3.12, 2.90 Å), arginine (3.15, 3.33 Å) and glutamic acid (2.65, 2.64 Å). Likewise, the hydrophobic interactions occurred between the aliphatic and the heterocyclic amino acids such as isoleucine, valine, asparagine, and proline.

Lastly, the P4C-5P21 complex formed five hydrogen bonds through the active site of the aliphatic amino acids such as threonine (2.76, 2.74 Å), glycine (3.17 Å), and lysine (3.06, 2.78 Å). Also, the hydrophobic interactions formed between the aliphatic and the heterocyclic amino acids such as proline, alanine, glycine, and valine.

The ligand P5C showed binding energy of -5.53, -5.60, and -5.64 kcal mol^{-1} for binding to the target proteins 4DSU, 4Q21, and 5P21, respectively. The P5C-4DSU complex formed seven hydrogen bonds through the active sites of the amino acids in the binding pocket of the target proteins such as glycine (3.07 Å), lysine (2.89, 3.15 Å), asparagine (2.55, 2.74 Å), valine (2.99 Å) and proline (2.84 Å). Also, the hydrophobic interaction with amino acids glycine, serine, threonine, and alanine. The P5C-4Q21 complex formed seven hydrogen bonds through the active sites of amino acids such as glycine (2.94 Å), lysine (2.93 Å), valine (2.93 Å), glycine (3.21 Å) and tyrosine (2.90, 3.0, 2.60 Å). Likewise, the hydrophobic interactions formed between the amino acids such as valine, serine, alanine, proline, and glutamic acid. Finally, the P5C-5P21 complex formed 6 hydrogen bonds through the active sites of amino acids such as lysine (2.87, 2.67 Å), valine (2.68 Å), glycine (2.98 Å), alanine (2.94 Å), and threonine (2.91 Å). Also, the hydrophobic interactions formed between glycine, serine, and proline. According to Table 8, the molecular docking interactions between the ligands and proteins were facilitated by the hydroxyl (-OH) and aldehydes (-CHO) functional groups of the pyrogallol carboxaldehyde, and the amino ($-NH_2$) and carboxylic (-COOH) functional groups of amino acids through hydrogen bonds. The ligands of the pyrogallol carboxaldehyde exhibited the same effects on the oncogenic proteins, making them promising targets in the advancement of anti-tumour drugs.

CONCLUSION

In this study, the presence of the electronegative oxygen atom in pyrogallol carboxaldehydes resulted in the elongation of the C_5-C_{11} bond. This was due to the ability of oxygen atom to pull the electrons from the carbon (C_{11}), resulting in a longer and weaker bond. The high polarizability and potent bioactivity of these compounds were supported by their chemical hardness and chemical potential. As demonstrated by the MESP and Mulliken charge distributions, the proximity of the aldehyde and hydroxyl group influenced the charges of the carbon atoms. The ADME predictions suggested that the pyrogallol carboxaldehydes had advantageous pharmacological characteristics that satisfied the Lipinski's criterion, confirming their bioavailability as a promising therapeutic agent. In molecular docking, the interactions between the ligands and proteins occurred through hydrogen bonds involving the hydroxyl and the aldehyde functional groups of pyrogallol carboxaldehyde, and the amino and carboxylic functional groups of amino acids. The binding affinity values of the pyrogallol carboxaldehydes showed that the P4C had the highest effectiveness on 4Q21 with a binding energy of -5.52 kcal mol^{-1}. Similarly, the P5C showed remarkable effectiveness on 5P21 with a binding energy of -5.64 kcal mol^{-1}. These findings highlight that these compounds act as potent inhibitors against oncogenic proteins, representing their strong anti-tumour activity.

REFERENCES

[1] Balachandran, V.; Karpagam, V.; Lakshmi, A., Conformational stability, theoretical and experimental vibrational spectral analysis of 2,4,6-trihydroxybenzaldehyde. *J. Mol. Struct*. **2012**, *1021*, 13-21, DOI: 10.1016/j.molstruc.2012.04.070.

[2] Alamri, A.; El-Newehy, M. H.; Al-Deyab, S. S., Biocidal polymers synthesis and antimicrobial properties of benzaldehyde derivatives immobilized onto amine-terminated polyacrylonitrile. *Chem. Cent. J.* **2012**, *6*, 111, DOI: 10.1186/1752-153X-6-111.

[3] Aslam, K.; Khosa, M. K.; Jahan, N.; Nosheen, S., Short communication synthesis and applications of Coumarin. *Pak. J. Pharm. Sci.* **2010**, *23*, 449-454.

[4] Rafiee, M.; Javaheri, M., A theoretical study of benzaldehyde derivatives as tyrosinase inhibitors using ab initio calculated NQCC parameters. *Mol. Biol. Res. Commun.* **2015**, *4*, 151-159.

[5] Ksendzova, G. A.; Samovich, S. N.; Sorokin, V. L.; Shadyro, O. I., Effects of hydroxylated benzaldehyde derivatives on radiation-induced reactions involving various organic radicals. Radiat. *Phys. Chem.* **2018**, *146*, 115-120, DOI: 10.1016/ j.radphyschem.2018.01.012.

[6] Batra, P.; Sharma, A. K., Anti-cancer potential of flavonoids: recent trends and future perspectives. *3 Biotech,* **2013**, *3,* 439-459, DOI: 10.1007/s13205-013-0117-5

[7] Thirunavukkarasu, K.; Rajkumar, P.; Selvaraj, S.; Suganya, R.; Kesavan, M.; Gunasekaran, S.; Kumaresan, S., Vibrational (FT-IR and FT-Raman), electronic (UV-Vis), NMR (^{1}H and ^{13}C) spectra and molecular docking analyses of anticancer molecule 4-hydroxy-3-methoxycinnamaldehyde. *J. Mol. Struct*. **2018**, *1173*, 307-320, DOI: 10.1016/ j.molstruc.2018.07.003.

[8] Ram Kumar, A.; Selvaraj, S.; Jayaprakash, K. S.; Gunasekaran, S.; Kumaresan, S.; Devanathan, J.; Selvam, K. A.; Ramadass, L.; Mani, M.; Rajkumar, P., Multi-spectroscopic (FT-IR, FT-Raman, ^{1}H NMR and ^{13}C NMR) investigations on syringaldehyde. *J. Mol. Struct.* **2021**, 1229, 129490, DOI: 10.1016/ j.molstruc.2020.129490.

[9] Rajkumar, P.; Selvaraj, S.; Suganya, R.; Kesavan, M.; Serdaroglu, G.; Gunasekaran, S.; Kumaresan, S., Experimental and theoretical investigations on electronic structure of 5-(hydroxymethyl)-2-furaldehyde: An antisickling agent identified from terminalia bellirica. *Chem. Data Collect*, **2020**, *29*, 100498, DOI: 10.1016/j.cdc.2020.100498.

[10] Kim, B. K.; Cho, J. H.; Jeong, P.; Lee, Y.; Lim, J. J.; Park, K. R.; Eom, S. H.; Kim, Y. C., Benserazide, the first allosteric inhibitor of Coxsackievirus B3 3C protease. *FEBS Lett.* **2015**, *589*, 1795-1801, DOI: 10.1016/j.febslet.2015.05.027.

[11] Kim, J. B.; Cho, K. J.; König, G. M.; Wright, A. D., Antioxidant activity of 3,4,5-trihydroxybenzaldehyde isolated from Geum japonicum. *J. Food. Drug. Anal.* **2006**, *14*, 13, DOI: 10.38212/2224-6614.2492.

[12] Kaur, B.; Kumar, S.; Kaushik, B. K., Recent advancements in optical biosensors for cancer detection. Biosens. *Bioelectron.* **2022**, *197*, 113805, DOI: 10.1016/j.bios.2021.113805.

[13] Luo, J.; Solimini, N. L.; Elledge, S. J., Principles of cancer therapy: oncogene and non-oncogene addiction. *Cell*, **2009**, *136*, 823-837, DOI: 10.1016/ j.cell.2009.02.024.

[14] Gokce, H.; Sen, F.; Sert, Y.; Abdel-Wahab, B. F.; Kariuki, B. M.; El-Hiti, G. A., Quantum computational investigation of (E)-1-(4-methoxyphenyl)-5-methyl-N′-(3-phenoxybenzylidene)-1H-1,2,3-triazole-4-carbohydrazide. *Molecules*, **2022**, *27* (7), 2193, DOI: 10.3390/molecules27072193.

[15] Sert, Y.; Gumus, M.; Gokce, H.; Kani, I.; Koca, İ., Molecular docking, Hirshfeld surface, structural, spectroscopic, electronic, NLO and thermodynamic analyses on novel hybrid compounds containing pyrazole and coumarin cores. *J. Mol. Struct*. **2018**, *1171,* 850-866, DOI: 10.1016/j.molstruc.2018.06.069.

[16] Abdulridha, A. A.; Allah, M. A. A. H.; Makki, S. Q.; Sert, Y.; Salman, H. E.; Balakit, A. A., Corrosion inhibition of carbon steel in 1 M H_2SO_4 using new Azo Schiff compound: Electrochemical, gravimetric, adsorption, surface and DFT studies. *J. Mol. Liq.* **2020**, *315*, 113690, DOI: 10.1016/ j.molliq.2020.113690.

[17] Nayak, A. K., Bismuth-Based Materials for Environmental Remediation. *IOP Publishing*, **2022**, p. 1-33, DOI: 10.1088/978-0-7503-5138-6.

[18] Chang, J. H.; Kumar, M.; Nayak, A. K., Nanostructured materials for photoelectrochemical water splitting. *IOP Publishing*, **2021**, p. 1-20, DOI: 10.1088/978-0-7503-3699-4.

[19] Nayak, A. K.; Sahu, N. K., *Nanostructured materials for visible light photocatalysis*, Elsevier, **2021**, p.1-609, DOI: 10.1016/C2019-0-05075-3.

[20] Kohn, W.; Sham, L. J., Self-consistent equations including exchange and correlation effects. *Phys. Rev.* **1965**, *140*, A1133-A1138, DOI: 10.1103/ PhysRev.140.A1133.

[21] Becke, A. D., Density functional thermo chemistry-III: The role of exact exchange. *J. Chem. Phys.* **1993**, *98*, 5648-5652, DOI: 10.1063/1.464913.

[22] Lee, C.; Yang, W.; Parr, R. G., Development of the Colle-Salvetti correlation-energy formula into a functional of the electron density. *Phys. Rev. B.* **1988**,

37, 785-789, DOI: 10.1103/PhysRevB.37.785.

[23] Frisch, M. J., *et al.*, Gaussion 09W, Revision A.02, Gaussion Inc. Walling Ford, CT, **2009.**

[24] Zhurko, G. A.; Zhurko, D. A., 2009 Chemcraft Program Version 1.6 (Build 315), http://www.chemcraftprog.com

[25] Thomas, L.; Mathew, S.; Johnson, S., *In-silico* prediction of role of chitosan, chondroitin sulphate and agar in process of wound healing towards scaffold development. *Inform. Med. Unlocked.* **2020**, *20*, 100406, DOI: 10.1016/j.imu.2020.100406.

[26] DeLano, W. L., Pymol: An open-source molecular graphics tool. CCP4 News letter on protein Crystallography, **2002**, *40*, 82-92, http://www.pymol.org.

[27] Denningten, R.; Keith, T.; Millam, J., GaussView Version 5.0.8 (Wallingford, CT: Gaussian, Inc, **2009**, 235.

[28] Morris, G. M.; Huey, R.; Lindstrom, W.; Sanner, M. F.; Belew, R. K.; Goodsell, D. S.; Olson, A. J., AutoDock4 and AutoDockTools4: Automated docking with selective receptor flexibility. *J. Comput. Chem.* **2009**, *30*, 2785-2791, DOI: 10.1002/jcc.21256.

[29] Wallace, A. C.; Laskowski, R. A.; Thornton, J. M., LIGPLOT: a program to generate schematic diagrams of protein-ligand interactions, *Protein Eng.* **1995**, *8*, 127-134, DOI: 10.1093/protein/8.2.127.

[30] Kim, B. K.; Ko, H.; Jeon, E. S.; Ju, E. S.; Jeong, L. S.; Kim, Y. C., 2,3,4-Trihydroxybenzyl-hydrazide analogues as novel potent coxsackievirus B3 3C protease inhibitors. *Eur. J. Med. Chem.* **2016**, *120*, 202-216, DOI: 10.1016/j.ejmech.2016.03.085.

[31] Zhao, J.; Khan, I. A.; Fronczek, F. R., Gallic acid. *Acta. Crystallogr. Sect. E. Struct. Rep. Online.* **2011**, *67*, o316-o317, DOI: 10.1107/S1600536811000262.

[32] Arunpandian, R.; Lasalle, B. S. I.; Balagowtham, N.; Krishnamachari, M.; Pandian, M. S.; Ramasamy, P.; Mohanraj, K.; Chiang, C. H.; Yang, P. Y., Computational and experimental investigation on piperazinediium bis (4-aminobenzoate) dihydrate single crystal for NLO applications. *J. Mol. Struct*. **2023**, *1288*, 135811, DOI: 10.1016/j.molstruc.2023.135811.

[33] Huang, C. Y.; Kumar, M.; Selvaraj, P.; Subramani, K.; Srinivasan, B.; Hsu, C. J., Fast-response liquid crystal lens with doping of organic N-benzyl-2-methyl-4-nitroaniline. *Opt. Express*. **2020**, *28* (7), 10572-10582, DOI: 10.1364/OE.390001.

[34] Selvaraj, S.; Ram Kumar, A.; Ahilan, T.; Kesavan, M.; Gunasekaran, S.; Kumaresan, S., Multi spectroscopic and computational investigations on the electronic structure of oxyclozanide. *J. Indian Chem. Soc.* **2022**, *99* (10), 100676, DOI: 10.1016/j.jics.2022.100676.

[35] Daina, A.; Michielin, O.; Zoete, V., SwissADME: a free web tool to evaluate pharmacokinetics, drug-likeness and medicinal chemistry friendliness of small molecules. *Sci. Rep.* **2017,** *7*, 42717, DOI: 10.1038/srep42717.

[36] Dege, N.; Gokce, H.; Dogan, O. E.; Alpaslan, G.; Agar, T.; Muthu, S.; Sert, Y., Quantum computational, spectroscopic investigations on N-(2-((2-chloro-4,5-dicyanophenyl) amino) ethyl)-4-methylbenzene-sulfonamide by DFT/TD-DFT with different solvents, molecular docking and drug-likeness researches. *Colloids Surf. A: Physicochem. Eng. Asp.* **2022**, *638*, 128311, DOI: 10.1016/j.colsurfa.2022.128311.

[37] Gumus, M.; Babacan, S. N.; Demir, Y.; Sert, Y.; Koca, I.; Gulcin, I., Discovery of sulfadrug-pyrrole conjugates as carbonic anhydrase and acetylcholinesterase inhibitors. *Archiv. Der Pharmazie*, **2022**, *355* (1), 2100242.